THE JOURNAL OF BIOLOGICAL CHEMISTRY VOL. 287, NO. 16, pp. 13336–13347, April 13, 2012
© 2012 by The American Society for Biochemistry and Molecular Biology, Inc. Published in the U.S.A.

Environment of Tyr_Z in Photosystem II from *Thermosynechococcus elongatus* in which PsbA2 Is the D1 Protein[S]

Received for publication, January 6, 2012, and in revised form, February 16, 2012 Published, JBC Papers in Press, February 23, 2012, DOI 10.1074/jbc.M112.340323

Miwa Sugiura[‡§¶1,2], Shogo Ogami[¶], Mai Kusumi[¶], Sun Un[‖], Fabrice Rappaport[**], and Alain Boussac[‖2]

*From the [‡]Cell-Free Science and Technology Research Center, Ehime University, Bunkyo-cho, Matsuyama, Ehime 790-8577, Japan, [§]PRESTO, Japan Science and Technology Agency (JST), 4-1-8, Honcho, Kawauchi, Saitama 332-0012, Japan, the [¶]Department of Chemistry, Graduate School of Science and Technology, Ehime University, Bunkyo-cho, Matsuyama, Ehime 790-8577, Japan, [‖]iBiTec-S, CNRS UMR 8221, CEA Saclay, 91191 Gif-sur-Yvette, France, and the **Institut de Biologie Physico-Chimique, CNRS UMR 7141 and Université Pierre et Marie Curie, 13 rue Pierre et Marie Curie, 75005 Paris, France*

Background: Photosystem II, the water-splitting enzyme, includes a protein, D1, which can be coded by three different *psbA* genes in *Thermosynechococcus elongatus.*
Results: In PsbA2-PSII, the environment of Tyr_Z is different from that in PsbA1-PSII and PsbA3-PSII.
Conclusion: The geometry of the Tyr_Z-O···H···Nϵ-His-190 bonding is an important parameter for PSII activity.
Significance: The environment of the cofactors is involved in the tuning of the electron transfer efficiency.

The main cofactors that determine the photosystem II (PSII) oxygen evolution activity are borne by the D1 and D2 subunits. In the cyanobacterium *Thermosynechococcus elongatus*, there are three *psbA* genes coding for D1. Among the 344 residues constituting D1, there are 21 substitutions between PsbA1 and PsbA3, 31 between PsbA1 and PsbA2, and 27 between PsbA2 and PsbA3. Here, we present the first study of PsbA2-PSII. Using EPR and UV-visible time-resolved absorption spectroscopy, we show that: (i) the time-resolved EPR spectrum of $\mathrm{Tyr}_Z^{\bullet}$ in the $(\mathrm{S}_3\mathrm{Tyr}_Z^{\bullet})'$ is slightly modified; (ii) the split EPR signal arising from $\mathrm{Tyr}_Z^{\bullet}$ in the $(\mathrm{S}_2\mathrm{Tyr}_Z^{\bullet})'$ state induced by near-infrared illumination at 4.2 K of the $\mathrm{S}_3\mathrm{Tyr}_Z$ state is significantly modified; and (iii) the slow phases of $\mathrm{P}_{680}{}^{+}$ reduction by Tyr_Z are slowed down from the hundreds of μs time range to the ms time range, whereas both the $\mathrm{S}_1\mathrm{Tyr}_Z^{\bullet} \rightarrow \mathrm{S}_2\mathrm{Tyr}_Z$ and the $\mathrm{S}_3\mathrm{Tyr}_Z^{\bullet} \rightarrow \mathrm{S}_0\mathrm{Tyr}_Z + \mathrm{O}_2$ transition kinetics remained similar to those in PsbA(1/3)-PSII. These results show that the geometry of the Tyr_Z phenol and its environment, likely the Tyr-O···H···Nϵ-His bonding, are modified in PsbA2-PSII when compared with PsbA(1/3)-PSII. They also point to the dynamics of the proton-coupled electron transfer processes associated with the oxidation of Tyr_Z being affected. From sequence comparison, we propose that the C144P and P173M substitutions in PsbA2-PSII *versus* PsbA(1/3)-PSII, respectively located upstream of the α-helix bearing Tyr_Z and between the two α-helices bearing Tyr_Z and its hydrogen-bonded partner, His-190, are responsible for these changes.

Light-driven water oxidation catalyzed by photosystem II (PSII)[3] is the first step in the photosynthetic production of biomass, fossil fuels, and O_2 on earth. Refined three-dimensional x-ray structures from 3.5 to 2.9 Å resolution have been obtained using PSII isolated from the thermophilic cyanobacterium *Thermosynechococcus elongatus* (1, 2). More recently, an x-ray structure at 1.9 Å resolution has been obtained using PSII isolated from the thermophilic cyanobacterium *Thermosynechococcus vulcanus* (3). PSII core complex is made up of 17 transmembrane protein subunits and 3 extrinsic proteins. In total, it contains 35 chlorophylls, 2 pheophytins, 2 hemes, 1 non heme iron, 2 quinones, 3–4 calcium ions, one of which is part of the $\mathrm{Mn}_4\mathrm{CaO}_5$ cluster, 3 chloride ions, two of which are at 7 Å from the $\mathrm{Mn}_4\mathrm{CaO}_5$ cluster, 11–12 carotenoid molecules, more than 20 lipids, and over 1300 water molecules (3).

The main cofactors involved in the function of PSII are integral components of the D1 and D2 proteins. The exciton resulting from the absorption of a photon is transferred to the photochemical trap, which undergoes a charge separation. The positive charge is then stabilized on P_{680}, a weakly coupled chlorophyll dimer (P_{D1} and P_{D2}). Then, $\mathrm{P}_{680}{}^{+}$ oxidizes a tyrosine residue of the D1 polypeptide, Tyr_Z, which in turn oxidizes the $\mathrm{Mn}_4\mathrm{CaO}_5$ cluster. On the acceptor side, the pheophytin anion ($\mathrm{Pheo}_{\mathrm{D1}}{}^{-}$) transfers the electron to the primary quinone electron acceptor, Q_A, which in turn reduces the second quinone, Q_B. Q_A is tightly bound and acts as a one-electron carrier, whereas Q_B acts as a two-electron and two-proton acceptor with a stable semiquinone intermediate, $\mathrm{Q}_B^{\bullet -}$. Although the Q_B^{-} semiquinone state is tightly bound, the quinone and quinol forms are exchangeable with the quinone pool in the thylakoid membrane (*e.g.* Refs. 4–9).

[S] This article contains supplemental Figs. S1–S7.

[1] Supported by the JST-PRESTO program (4018) and Grant-in-aid for Scientific Research 21612007 from the Ministry of Education, Science, Sports, Culture and Technology. To whom correspondence may be addressed: Cell-Free Science and Technology Research Center, Ehime University, Bunkyo-cho, Matsuyama Ehime 790-8577, Japan. E-mail: miwa.sugiura@ehime-u.ac.jp.

[2] To whom correspondence may be addressed. E-mail: alain.boussac@cea.fr.

[3] The abbreviations used are: PSII, photosystem II; Chl, chlorophyll; PPBQ, phenyl-*p*-benzoquinone, P_{680}, chlorophyll dimer acting as the second electron donor; Q_A, primary quinone acceptor; Q_B, secondary quinone acceptor; $\mathrm{Pheo}_{\mathrm{D1}}$, pheophytin P_{D1} and P_{D2}; NIR, near-infrared; P_{D1} and P_{D2}, Chl monomers of P_{680} on the D1 and D2 side, respectively.

The Mn_4CaO_5 cluster acts both as a device accumulating oxidizing equivalents and as the catalytic site for water oxidation. The enzyme cycles sequentially through five redox states, denoted S_n, where n stands for the number of oxidizing equivalents stored. Upon formation of the S_4 state, two molecules of water are rapidly oxidized, the S_0 state is regenerated, and O_2 is released (10, 11).

Cyanobacterial species have multiple *psbA* variants coding for the D1 protein (*e.g.* Refs. 12–20). These different genes are known to be differentially expressed depending on the environmental conditions (*e.g.* Refs. 12–18). In particular, specific up/down-regulations of one of these genes under high light conditions is indicative of a photo-protection mechanism. For example, the mesophilic cyanobacterium, *Synechocystis* PCC 6803, has three *psbA* genes. Two of these (*psbAII* and *psbAIII*) produce an identical D1. Nevertheless, although *psbAII* is expressed under the "normal" cultivation conditions, transcription of *psbAIII* is induced by high light or UV light (15), and that of *psbAI* seems triggered by microaerobic conditions (18). *T. elongatus* also has three different *psbA* genes in its genome (20). The comparison of the mature D1 amino acid sequence deduced from the *psbA₃* gene with those of the *psbA₁* and *psbA₂* genes points to a difference of 21 and 31 residues, respectively (see supplemental Figs. S1 and S2). It has been reported that in *T. elongatus*, *psbA₁* is constitutively expressed under normal laboratory conditions, whereas the transcription of *psbA₃* occurred under high light or UV light conditions (16, 21, 22).

In *T. elongatus*, the change of Q130 in PsbA1-PSII to E130 in PsbA3-PSII has been shown to increase the midpoint potential of $Pheo_{D1}/Pheo_{D1}^{\bar{\cdot}}$ by 17 mV from −522 mV in PsbA1-PSII (23) to −505 mV in PsbA3-PSII (19). Because this increase was half the one observed upon single site-directed mutagenesis in *Synechocystis* PCC 6803 (24, 25), this led us to propose that the effects of the D1-Q130E substitution could be, at least partly, compensated for by some of the additional amino acid changes associated with the PsbA3 for PsbA1 substitution (19). For manganese-depleted PSII and above pH 7.5, where the phenolic hydroxyl group of Tyr_Z hydrogen-bonds H190, the proton acceptor, Tyr_Z oxidation by $P_{680}^{\dot{+}}$ is controlled by its prior deprotonation (26), and the electron transfer rate between $P_{680}^{\dot{+}}$ and Tyr_Z has been found to be slightly faster in PsbA3-PSII (global $t_{1/2}$ ~100 μs) than in PsbA1-PSII (global $t_{1/2}$ ~200 μs (19). The temperature dependences of the $S_2Q_A^{\bar{\cdot}}$ charge recombination in PsbA1 and PsbA3 have shown that the environments of Q_A and, as a consequence, its redox potential, are likely to be different (19). The exchange of S270 in PsbA1 for A270 in PsbA3 has been suggested to influence the stabilization of the sulfoquinovosyl-diacylglycerol molecule that lies between Q_B and nonheme iron (27). Maybe as a consequence, the binding of bromoxynil in PsbA3-PSII and in PsbA1-PSII has been found to differ, suggesting that the Q_B pocket had different properties. It has been also found that the midpoint potential of the Fe^{III}/Fe^{II} couple was likely higher in PsbA1-PSII than in PsbA3-PSII (28). In addition, under photo-inhibitory conditions, the accelerated decrease in O_2 evolution in WT*1 [4] (producing PsbA1-PSII) cells was found to correlate with a much faster inhibition of the S_2 state formation than in WT*3 (producing PsbA3-PSII) cells (29).

Although there have been an increasing number of studies aimed at characterizing the properties of PsbA1-PSII when compared with those of PsbA3-PSII, those of PsbA2-PSII have not yet been reported. In the present work, we describe the first construction of a *T. elongatus* deletion mutant lacking both the *psbA₁* and the *psbA₃* genes and expressing only *psbA₂*. We focused our first characterization of PsbA2-PSII on the electron transfer reactions involving Tyr_Z. Using continuous wave EPR at helium temperature, time-resolved EPR at room temperature, and time-resolved UV-visible absorption spectroscopy, it is shown that the properties of Tyr_Z are modified in PsbA2-PSII when compared with those in Psb(A1/3)-PSII.

EXPERIMENTAL PROCEDURES

Construction of T. elongatus Mutants—The construction of the Δ*psbA₁*Δ*psbA₂* *T. elongatus* deletion mutant (WT*3) from a *T. elongatus* 43-H strain that had a His_6 tag on the C terminus of CP43 (32) has been previously described in Ref. 33.

For making the Δ*psbA₁*Δ*psbA₃* *T. elongatus* deletion mutant (WT*2) (Fig. 1), first, the *psbA₁* gene and its promoter region (~180 bp) were substituted together from the 43-H strain with a chloramphenicol-resistant cassette (~1300 bp) by using the plasmid vector pBΔ*psbA₂*. Then, the *psbA₃* gene was substituted with a spectinomycin/streptomycin resistance gene cassette (~2100 bp) by using the plasmid pBΔ*psbA₃*. For construction of pBΔ*psbA₁*, a DNA fragment of ~2300 bp of the *psbA₂* gene (*tlr1844*) including its promoter region (~180 bp) and the 3′-flanking region of *psbA₂* (~1000 bp) was cloned from *T. elongatus* wild-type genomic DNA by PCR amplification and subcloned into a plasmid vector pBluescript II SK+ at EcoRV and XhoI sites. Next, a chloramphenicol resistance gene cassette (~1300 bp) was ligated to the upstream of the *psbA₂* gene at BamHI and EcoRV of the plasmid DNA. Then, a separately amplified ~900-bp DNA fragment of the 3′-flanking region of *psbA₁* (but without the *psbA₁* promoter region) was ligated to the subcloned plasmid vector at SacI and BamHI. For the construction of pBΔ*psbA₃*, a DNA fragment of ~900 bp of the 3′-flanking region of the *psbA₃* (*tlr1477*) was cloned from *T. elongatus* wild-type genomic DNA by PCR amplification and subcloned into a plasmid vector pBluescript II SK+ between SacI and EcoRI sites. Then, a spectinomycin/streptomycin resistance gene cassette (~2100 bp) was inserted at PstI and SacI. Then, a separately amplified ~1100-bp DNA fragment of the 5′-flanking region of *psbA₃* was ligated to the subcloned plasmid vector at SphI and PstI.

The *T. elongatus* transformants were selected as single colonies on DTN agar plate containing appropriate antibiotics (25 μg ml^{-1} spectinomycin, 10 μg ml^{-1} streptomycin, 40 μg ml^{-1} kanamycin, and 5 μg ml^{-1} chloramphenicol). Segregation of all genome copies was confirmed by difference in length of amplified DNA by PCR using the *P1* primer (5′-GCTGTACTGGCCATCGCTGGGCACCACTCG-3′) and *P2* primer (5′-GGACTTATCACTACTTATCACTAGAGAGGT-3′) for *psbA₁*–*psbA₂* region, and using the *P3* primer (5′-GGTTGGATCCCCAGCCAGCGATCGCGGGAG-3′) and *P4* primer (5′-CCA-

---

[4] Throughout this study, WT*1, WT*2, and WT*3 are used to indicate cells containing only the *psbA₁*, *psbA₂*, and *psbA₃* gene, respectively.

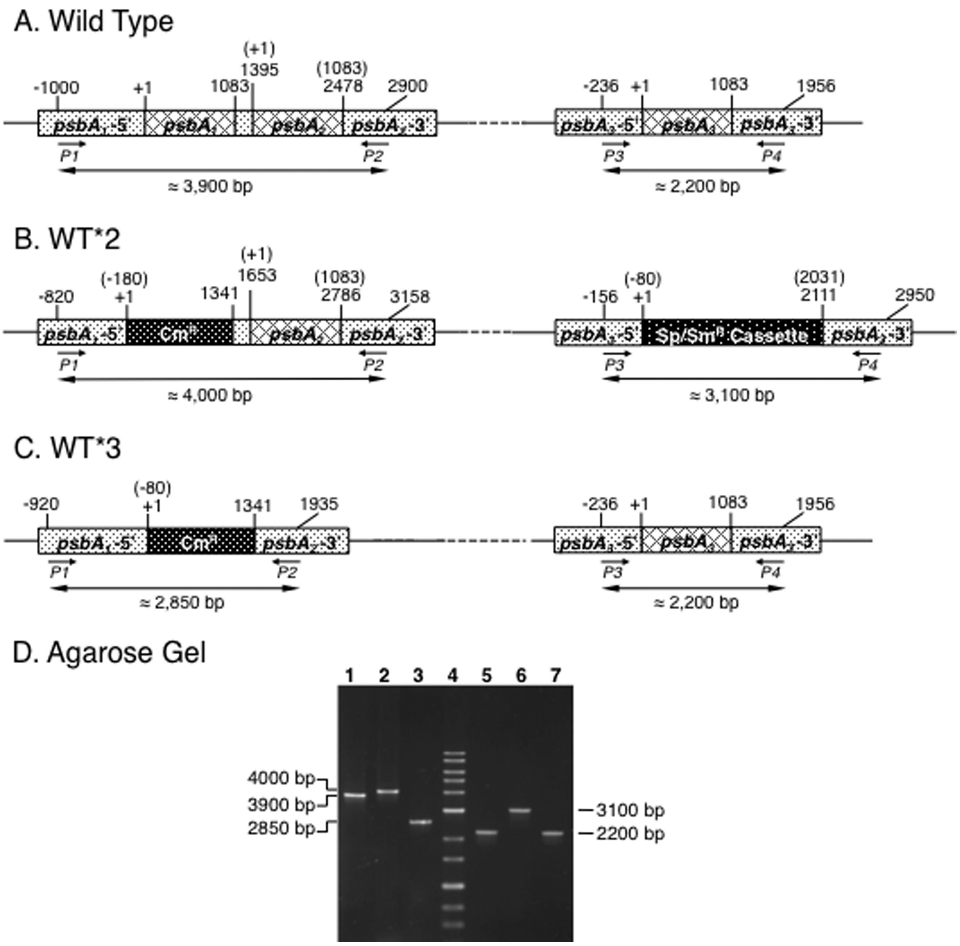

FIGURE 1. **Map around *psbA*$_1$ and *psbA*$_2$ and around *psbA*$_3$ in *T. elongatus* genome (*A–C*) and agarose gel electrophoresis of amplified products by PCR (*D*).** *A*, wild-type, all three *psbA* genes are intact. In *B*, for making WT*2, *psbA*$_1$ with 180 bp of the promoter region was deleted by substitution of a chloramphenicol-resistant (*Cm*^{R}) cassette, and *psbA*$_3$ was substituted by a spectinomycin (*Sp*)/streptomycin-resistant (*Sm*^{R}) cassette. In *C*, for making WT*3, both *psbA*$_1$ and *psbA*$_2$ were substituted by a chloramphenicol-resistant cassette. Primers are shown as *short arrows*, and *P1*, *P2*, *P3*, and *P4* indicate annealing position on their *T. elongatus* genome DNA. The *double-pointed arrows* show the length of the DNA amplified by PCR with using the appropriate primers. *D*, agarose gel (1%) electrophoresis of amplified products by PCR using *P1* and *P2* primers (*lanes 1–3*) and using *P3* and *P4* primers (*lanes 5–7*). *Lanes 1* and *5* correspond to the wild type; *lanes 2* and *6* correspond to the WT*2 strain; *lanes 3* and *7* correspond to the WT*3 strain; and *lane 4* corresponds to a 1-kb ladder marker (Toyobo).

TGCCCGCAAAACAGC-3′) for *psbA*$_3$ region as shown in Fig. 1. Complete segregation of the deletion mutants was confirmed by PCR amplification as shown in Fig. 1*D*. In the wild type, a 3900-bp DNA fragment including both *psbA*$_1$ and *psbA*$_2$ was amplified by *P1* and *P2* primers (*lane 1*). In contrast, a 4000-bp fragment (*lane 2*) and a 2850-bp fragment (*lane 3*) were amplified with using the same combination of the primers in WT*1 and WT*3, respectively. In the region of *psbA*$_3$, a 2200-bp fragment was amplified with *P3* and *P4* primers in both wild-type and WT*3 genomes (*lanes 5* and *7*), whereas a 3100-bp fragment was amplified in WT*2 genome (*lane 6*).

Purification of PSII—PSII were purified with the protocol already described (28). PSII samples were suspended in 1 M betaine, 10% glycerol, 15 mM $CaCl_2$, 15 mM $MgCl_2$, 40 mM MES, pH 6.5 adjusted with NaOH. For the low temperature X-band EPR experiments, glycerol was omitted because its presence decreases the yield of the near-infrared induced split EPR signal in the S_3 state.

For manganese depletion, PSII samples were diluted ~10-fold in a medium containing 1.2 M Tris-HCl (pH 9.2) and were incubated under room light at 4 °C for 1 h. The samples were collected by centrifugation (15 min at 170, 000 × *g*) after the addition of 1.2 M Tris (pH 9.2) containing 50% (w/v) polyethylene glycol 8000 so that the final PEG concentration was 12%. The pellet was resuspended in a medium containing 1 M betaine, 10% glycerol, 15 mM $CaCl_2$, 15 mM $MgCl_2$, 40 mM MES, pH 6.5 adjusted with NaOH, and 12% PEG. After a new centrifugation, the pellet was resuspended in 1 M betaine, 10% glycerol, 15 mM $CaCl_2$, 15 mM $MgCl_2$, 40 mM MES, pH 6.5 adjusted with NaOH.

Oxygen Evolution Measurements—Oxygen-evolving activity of purified PSII (5 μg of Chl ml^{-1}) was measured under continuous saturating white light at 25 °C by polarography using a Clark type oxygen electrode (Hansatech). A total of 0.5 mM 2,6-dichloro-*p*-benzoquinone (dissolved in dimethyl sulfoxide) was added as an electron acceptor.

EPR Spectroscopy—For helium temperature measurements, continuous wave EPR spectra were recorded with a Bruker Elexsys 500 X-band spectrometer equipped with a standard ER 4102 (Bruker) X-band resonator, a Bruker teslameter, an Oxford Instruments cryostat (ESR 900), and an Oxford ITC504 temperature controller. Flash illumination at room temperature was provided by a neodymium:yttrium-aluminum garnet laser (532 nm, 550 mJ, 8-ns Spectra Physics GCR-230–10). PSII samples at 1.1 mg of Chl ml^{-1} were loaded in the dark into quartz EPR tubes and dark-adapted for 1 h at room temperature. Then, the samples were synchronized in the S_1 state with one pre-flash (34). After a further 1-h dark adaptation at room temperature and the addition of 0.5 mM PPBQ dissolved in dimethylsulfoxide, the samples were either frozen immediately to 198 K in a solid CO_2/ethanol bath or illuminated by one or two additional flashes to generate the S_2 and S_3 states before being frozen in the dark to 198 K and then transferred to 77 K. In both cases, the samples were degassed at 198 K prior to the recording of the spectra.

For time-resolved measurements at room temperature, the spectrometer was equipped with a Super High Quality Bruker cavity. Saturating laser flash illumination at room temperature was provided by the laser described above. PSII at 1.1 mg of Chl ml^{-1} was loaded into a small volume flat cell (100 μl) in the presence of 0.5 mM phenyl-*p*-benzoquinone (PPBQ) and 1 mM potassium ferricyanide. Ferricyanide was added to avoid any contamination from the $PPBQ^{\bar{\cdot}}$ signal, which is detectable in the hundred μs time range after the flash illumination in the absence of ferricyanide. Formation and decay of the signal following laser flash illumination were measured at 32 magnetic field positions spread over 50 G and centered on the $Tyr_Z^{\bullet}$ EPR signal. For each of the 32 magnetic field values, 16 scans were averaged. The two-dimensional spectra (time *versus* field) of ~12–16 samples were averaged. Half of the two-dimensional spectra were obtained by increasing the magnetic field, and the other half were obtained by decreasing the magnetic field. When indicated, near-IR illumination of the samples was done directly in the EPR cavity and was provided by a laser diode emitting at 820 nm (Coherent, diode S-81-1000C) with a power of 600–700 milliwatts at the level of the sample.

The High Field-EPR measurements were taken on a locally built spectrometer described previously (35). Using a manganese-doped magnesium oxide sample, we verified that the relative accuracy of the magnetic field was better than 1 millitesla in the field ranges used in this study. The microwave frequency was accurate to better than 1 MHz. Hence, the measurement accuracy in g was expected to be 1×10^{-4}.

UV-visible Absorption Change Spectroscopy—Absorption changes were measured with a lab-built spectrophotometer (36) where the absorption changes are sampled at discrete times by short flashes. These flashes were provided by a neodymium:yttrium-aluminum garnet (355 nm) pumped optical parametric oscillator, which produces monochromatic flashes (1 nm full-width at half-maximum) with a duration of 5 ns. Excitation was provided by a second neodymium:yttrium-aluminum garnet (532 nm) pumped optical parametric oscillator, which produces monochromatic saturating flashes at 700 nm (1 nm full-width at half-maximum) with a duration of 5 ns. The path length of the cuvette was 2.5 mm. PSII was used at 25 μg of Chl ml^{-1} in 10% glycerol, 1 M betaine, 15 mM $CaCl_2$, 15 mM $MgCl_2$, and 40 mM MES (pH 6.5). PSIIs were dark-adapted for ~1 h at room temperature (20–22 °C) before the additions of 0.1 mM PPBQ dissolved in dimethyl sulfoxide. For kinetic measurements, the time delay between the actinic flash and the detector flash was first increased from the smaller value to the larger value and then varied in the opposite direction. For each time delay, the measurements were repeated four times so that each data point is the average of eight measurements. The traces shown are typical of those obtained with at least three different PSII preparations.

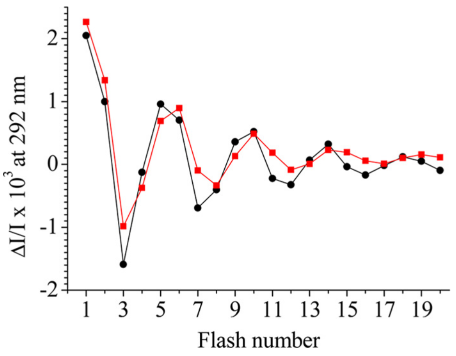

FIGURE 2. **Sequence of amplitude of absorption changes at 292 nm.** The measurements were done during a series of saturating flashes (spaced 200 ms apart) given to dark-adapted PsbA3-PSII (*black circles*) or PsbA2-PSII (*red squares*). The samples ([Chl] = 25 μg ml^{-1}) were dark-adapted for 1 h at room temperature before the addition of 100 μM PPBQ. The measurements were done 200 ms after each flash.

RESULTS

The oxygen evolution activity of purified PsbA2-PSII was 3000–3500 μmol of O_2 (mg of Chl)$^{-1}$ ml^{-1}. This activity is close to that found for PsbA1-PSII and about half of that commonly found for PsbA3-PSII (33).

Fig. 2 shows the amplitude of the absorption changes associated with each flash in a series with PsbA3-PSII (*circles*) and with PsbA2-PSII (*squares*). Measurements were done at 292 nm (37–39) and at 200 ms after the flashes, *i.e.* after completion of the reduction of Tyr_Z by the water-oxidizing complex. At this wavelength, the reduction of PPBQ does not lead to any absorption changes, and the successive oxidation steps of the water-oxidizing complex have significant extinction coefficients (38). The pattern, oscillating with a period of four, is clearly observed for both types of PSII preparations with very similar amplitude on the first flash. However, the damping is larger in PsbA2-PSII than in PsbA3-PSII. Indeed, the maxima are clearly shifted from the 5th, 9th, 13th, etc., flashes in PsbA3-PSII to the 6th, 10th, 14th, etc., flashes in PsbA2-PSII. This is at variance with the PsbA(1/3) cases, which displayed similar period four oscillation characteristics like the miss parameter and S_1/S_0 ratio in dark-adapted material (33, 39, 40). This suggests that functional differences exist between PsbA2-PSII and PsbA(1/3)-PSII.

To determine which step(s) is(are) kinetically affected and therefore responsible for the larger miss parameter in PsbA2-PSII, we first measured the absorption changes at 292 nm in the 10 μs to ms time ranges after the first three flashes in a series to assess the kinetics of electron transfer associated with the $S_1Tyr_Z^{\bullet} \rightarrow S_2Tyr_Z$, $S_2Tyr_Z^{\bullet} \rightarrow S_3Tyr_Z$ and $S_3Tyr_Z^{\bullet} \rightarrow S_0Tyr_Z$ transitions in both the PsbA2-PSII and the PsbA3-PSII. At 292 nm, the absorption changes associated with the $S_2Tyr_Z^{\bullet} \rightarrow S_3Tyr_Z$ transition are small and preclude a reliable kinetic analysis. As shown in Fig. 3, we did not observe any significant differences for the kinetics of the absorption changes associated

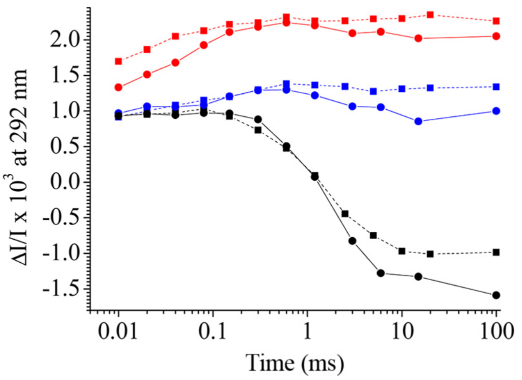

FIGURE 3. **Kinetics of absorption changes at 292 nm after first flash (*red*), second flash (*blue*), and third flash (*black*) given to dark-adapted PsbA3-PSII (*circles* and *continuous lines*) or PsbA2-PSII (*squares* and *dashed lines*).** Other experimental conditions were similar to those in Fig. 2.

with the $S_1Tyr_Z^{\bullet} \rightarrow S_2Tyr_Z$ and $S_3Tyr_Z^{\bullet} \rightarrow S_0Tyr_Z$ transitions in PsbA2-PSII (*squares*) when compared with PsbA3-PSII (*circles*). Thus, the larger miss parameter in PsbA2-PSII does not originate from a longer lifetime of the $S_iTyr_Z^{\bullet}$. In addition, we note that the light-induced absorption changes associated with the formation of the S_2 state were similar in PsbA2-PSII and PsbA3-PSII. This suggests a similar efficiency for the S_1 to S_2 transition. We aimed at verifying this conclusion by EPR spectroscopy that provides an exquisitely specific spectrum for the S_1 to S_2 transition.

Fig. 4*A* shows the difference EPR spectra "after-minus-before" flash illumination in PsbA3-PSII (*spectrum a*) and PsbA2-PSII (*spectrum b*). After one flash, the characteristic S_2 multiline signal centered at $g \sim 2$ and arising from the Mn_4CaO_5 cluster in the $Mn^{IV}{}_3Mn^{III}$ redox state with a spin state $S = 1/2$ (see Ref. 41 and references therein for a recent discussion) had an identical shape and a similar amplitude in PsbA3-PSII and PsbA2-PSII. In contrast, after two flashes (Fig. 4*B*), the amplitude of the S_2 multiline signal reflecting the fraction of water-oxidizing complex that did not undergo the $S_2 \rightarrow S_3$ transition was larger in PsbA2-PSII (*spectrum b*) than in PsbA3-PSII (*spectrum a*). The amplitude of the positive feature seen between 0 and 1000 G and assigned to the spin $S = 3$ S_3 signal (42) was smaller in PsbA2-PSII than in PsbA3-PSII. The temperature used (8.5 K) was not ideal to measure the S_3 EPR signal but was chosen to allow the detection of both the S_3 and the S_2 signals in the same spectrum. The two observations made above point to a lower yield of the S_2 to S_3 transition in PsbA2-PSII. Although the spectrum in PsbA2-PSII exhibits a larger negative signal in the nonheme iron magnetic field region at ~1100 G (*e.g.* Ref. 28), the shape of the signal assigned to S_3 was similar in both samples. This, together with the identical multiline signal observed in both samples, shows that the magnetic structure of the Mn_4CaO_5 cluster is likely unaffected by the substitution of PsbA3 by PsbA2.

We conclude from the above data that the larger miss parameter is not due to a longer lifetime of any of the $S_iTyr_Z^{\bullet}$ states that would result in a larger charge recombination probability. This makes the electron transfer step between $P_{680}{}^{+}$ and Tyr_Z the next candidate. Fig. 5*A* shows the time-resolved flash-induced absorption changes around 433 nm after each of the first five flashes applied to dark-adapted PsbA2-PSII (first flash, *black*; second flash, *blue*; third flash, *red*; fourth flash, *green*; fifth flash, *orange*). The spectra were recorded 20 ns after the flashes to avoid any spectral distortions due to the short lived excited state, like uncoupled Chl*, for example. In this spectral region, the redox changes of several species, such as the Chls, cytochromes, Tyr_Z, and Q_A, could potentially contribute to the absorption changes. The most prominent ones, however, are those associated with the formation of $P_{680}{}^{+}$. The $P_{680}{}^{+}/P_{680}$ difference spectrum is characterized by a strong Soret band bleaching. After one flash, *i.e.* in the $S_1P_{680}{}^{+}$ state, the maximum of the bleaching was observed at 433 nm. After the second flash and third flash, *i.e.* in the $S_2P_{680}{}^{+}$ state and $S_3P_{680}{}^{+}$ state, the width of the bleaching increased, and the red-most parts of the spectra were slightly red-shifted when compared with the spectrum of the $S_1P_{680}{}^{+}$ state. The red-shift was reversed after the fourth and fifth flashes, *i.e.* in the $S_0P_{680}{}^{+}$ and $S_1P_{680}{}^{+}$ states. This period four oscillation pattern in the $P_{680}{}^{+}/P_{680}$ spectrum likely originates from an electrostatic effect on the $P_{D1}{}^{+}P_{D2} \Leftrightarrow P_{D1}P_{D2}{}^{+}$ equilibrium due to the charge(s) stored on/around the Mn_4CaO_5 cluster (*e.g.* Ref. 4). Irrespective of the flash number, the difference spectra were similar to those in PsbA1-PSII (40) and PsbA3-PSII (33), thus showing that the distribution of the cation over the P_{D1} and P_{D2} chlorophylls is similar in both cases.

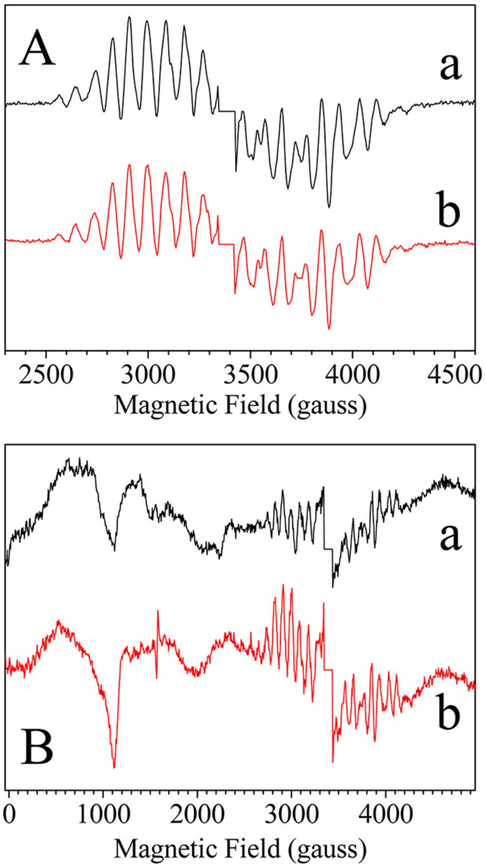

FIGURE 4. **Light-minus-dark EPR spectra induced by either one flash (*A*) or two flashes (*B*) at room temperature in presence of 0.5 mM PPBQ and recorded on PsbA3-PSII (*spectrum a, black*) or PsbA2-PSII (*spectrum b, red*).** Sample concentration was 1.1 mg of Chl ml⁻¹. Instrument settings were: modulation amplitude, 25 G; microwave power, 20 milliwatt; microwave frequency, 9.5 GHz; modulation frequency, 100 kHz; and temperature, 8.5 K. The central part of the spectra corresponding to the $Tyr_D{}^{\bullet}$ region was deleted.

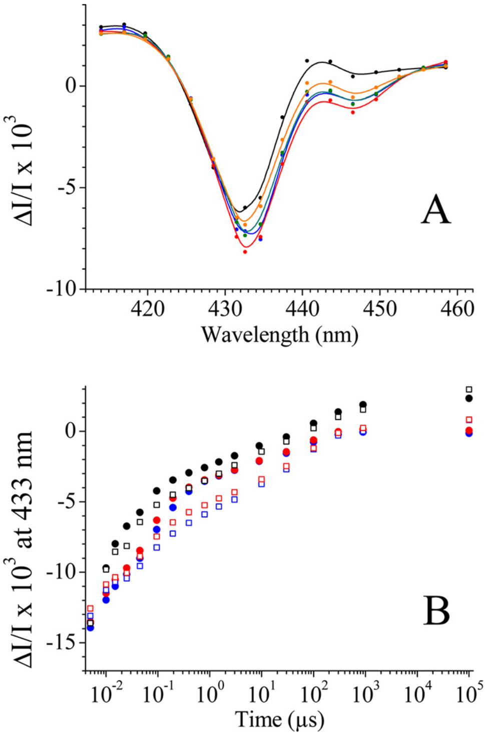

FIGURE 5. *A*, difference spectra around 430 nm. The flash-induced absorption changes were measured at 20 ns in PsbA2-PSII after the first five flashes given on dark-adapted PsbA2-PSII (first flash, *black*; second flash, *blue*; third flash, *red*; fourth flash, *green*; fifth flash, *orange*). [Chl] = 25 μg ml^{-1}. *B*, kinetics of $P_{680}^{+\bullet}$ reduction measured at 433 nm after the first three flashes in PsbA3-PSII (*filled circles*) and PsbA2-PSII (*open circles*). *Black circles*, first flash; *blue circles*, second flash; *red circles*, third flash.

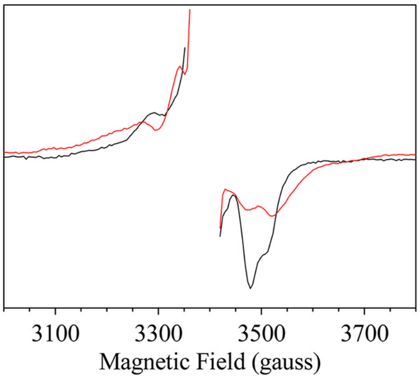

FIGURE 6. **NIR-induced split EPR spectra in PsbA3-PSII (*black spectrum*) and PsbA2-PSII (*red spectrum*).** For the two samples, a spectrum was first recorded after two flashes given at room temperature, and a second spectrum was recorded after a further NIR illumination given in the EPR cavity at 4.2 K. Instrument settings were: modulation amplitude, 25 G; microwave power, 20 milliwatt; microwave frequency, 9.5 GHz; modulation frequency, 100 kHz; and temperature, 4.2 K. The chlorophyll concentration was 1.1 mg ml^{-1}. The center part corresponding to the $Tyr_D^\bullet$ spectrum was deleted.

Fig. 5*B* shows the decay of $P_{680}^{+\bullet}$ measured at 433 nm after each of the first three flashes in PsbA3-PSII (*filled circles*) and PsbA2-PSII (*open circles*). After the first flash (*black symbols*), both the tens of ns and the tens of μs phases were found comparable in PsbA3-PSII and PsbA2-PSII in terms of amplitude and $t_{1/2}$. After the second flash (*blue symbols*) and the third flash (*red symbols*), the $P_{680}^{+\bullet}$ decay was much slower in PsbA2-PSII, particularly in the hundreds of μs time domain. This shows up even more clearly after averaging the decay traces from the 1st flash to the 20th flash (supplemental Fig. S6).

The finding that the reduction kinetics of $P_{680}^{+\bullet}$ is hardly affected on the first flash shows that possible changes of the properties of the electron acceptor side originating from the PsbA(1/3) to PsbA2 substitution did not significantly increase the percentage of centers in which the $P_{680}^{+\bullet}Q_A^{-\bullet}$ charge recombination occurred, at least with Q_B in the oxidized state. In addition, the presence of PPBQ prevents the formation of stable $Q_B^{-\bullet}$ so that the acceptor side is in the same redox state after each flash in the series. Therefore, it is very unlikely that the slower P_{680}^{+} reduction detected on the second and following flashes originates from a more efficient charge recombination in PsbA2-PSII.

According to the current understanding of the multiphasicity of the reduction of $P_{680}^{+\bullet}$, the ns components are kinetically limited by the electron transfer process, whereas the μs phases involve proton-coupled transfer reactions (*e.g.* Refs. 43–45). In this framework, the present data would thus point to a slower proton transfer process in PsbA2-PSII. Two amino acid substitutions on the electron donor side of PsbA2-PSII may affect the orientation of the helices, which respectively bear His-190 and $Tyr_Z^\bullet$: the C144P and P173M exchanges. These two substitutions may impact the hydrogen bond between Tyr_Z and His-190 and/or the H-bond network in which these two residues are involved. If such is indeed the case, this would be expected to affect the rates of the proton transfer steps associated with the oxidation of Tyr_Z. This was assessed using EPR spectroscopy, which has been shown to probe the geometry and the environment of the Tyr_Z phenol ring (*e.g.* Refs. 46 and 47).

In the S_3 state, NIR illumination at ~4 K results in the formation of a split EPR signal (48, 49), attributed to a $(S_2Tyr_Z^\bullet)'$ state formed by NIR-induced conversion of the manganese cluster into an "activated" state able to oxidize Tyr_Z and thus leading to the formation of $(S_2Tyr_Z^\bullet)'$ at the expense of the S_3Tyr_Z state (50). This split signal is attributed to the magnetic interaction between $Tyr_Z^\bullet$, with a spin state S = 1/2 and the Mn_4CaO_5 cluster possibly in a S = 7/2 spin state (51), and as such is very sensitive to the geometry of the $Tyr_Z^\bullet/Mn_4CaO_5$ ensemble. As an example of this sensitivity, the split EPR spectrum is significantly modified upon the Ca^{2+}/Sr^{2+} exchange (52). Importantly, these modifications can be reliably ascribed to changes in the geometry of the bridge between Tyr_Z and Ca^{2+}/Sr^{2+} via a water molecule (3) rather than to the alteration of the Mn_4CaO_5 magnetic structure, which has been independently shown to be only slightly affected by the Ca^{2+}/Sr^{2+} exchange (41).

Fig. 6 shows the EPR difference spectra after-minus-before near-infrared illumination in PsbA2-PSII (*red spectrum*), which are compared with that recorded in PsbA3-PSII (*black spectrum*). Notably, either PsbA1-PSII or PsbA3-PSII can be used as control samples because their split signals are identical (40, 49, 52). Fig. 6 evidences manifest differences between the two samples. Because the PsbA exchange does not modify the EPR properties of the Mn_4CaO_5 cluster, at least in the S_2 and S_3 states, the changes in the split signal likely arise from a change in the EPR properties of $Tyr_Z^\bullet$ or in the magnetic interaction between $Tyr_Z^\bullet$ and the Mn_4CaO_5 cluster. The EPR properties of $Tyr_Z^\bullet$ that may be modified are: (i) the values and localization of

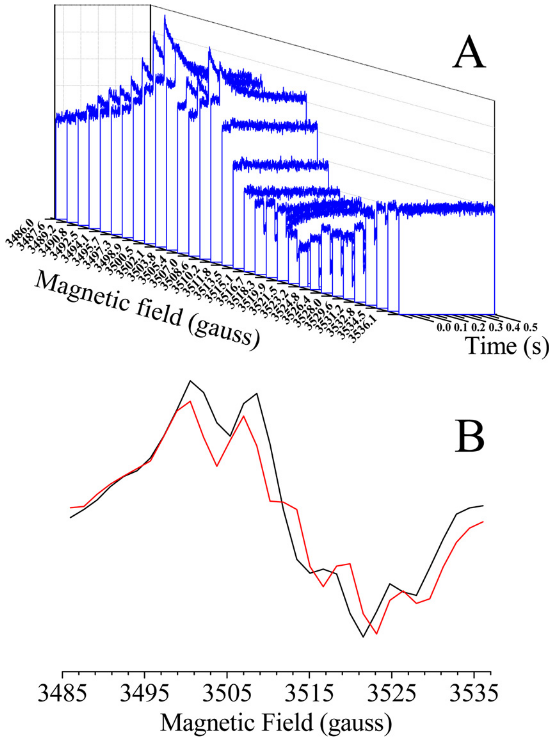

FIGURE 7. *A*, formation and decay of the $Tyr^{\bullet}$ signal following laser flash illumination of manganese-depleted PsbA3-PSII measured at 32 magnetic field positions spread over 50 G from 3486 to 3536 G. For each of the 32 magnetic field values, 16 scans were averaged. The two-dimensional spectra (time *versus* field) of ~12–16 samples were averaged. Half of the two-dimensional spectra was obtained by increasing the magnetic field, and the other half was obtained by decreasing the magnetic field. Other instrument settings; modulation amplitude, 4 G; microwave power, 20 milliwatt; microwave frequency, 9.7 GHz; modulation frequency, 100 kHz; and temperature, 293 K. The chlorophyll concentration was 1.1 mg ml^{-1}. Sampling time was 500 μs. *B*, $Tyr_D^{\bullet}$ (*black*) and $Tyr_Z^{\bullet}$ (*red*) spectra extracted from the two-dimensional spectrum in *panel A*. The $Tyr_D^{\bullet}$ spectrum is the envelope of the baseline before the flash, and the $Tyr_Z^{\bullet}$ spectrum was obtained by extracting the first slice after the flash (*i.e.* ~1 ms) after subtraction of the baseline before the flash, which corresponds to the $Tyr_D^{\bullet}$ spectrum.

the spin densities on the carbons and oxygen bearing this spin density; (ii) the orientation of the β-methylene group *versus* the plan of the phenol ring; (iii) the g_x, g_y, and g_z values; (iv) the relative orientation of $Tyr_Z^{\bullet}$ *versus* the Mn_4CaO_5 cluster; and (v) the distance between $Tyr_Z^{\bullet}$ and the Mn_4CaO_5 cluster. The changes in the magnetic interaction between $Tyr_Z^{\bullet}$ and the Mn_4CaO_5 cluster could be assessed by a theoretical approach. Nevertheless, although some of the split signals, in acetate-treated PSII or in the $S_1Tyr_Z^{\bullet}$ generated at 4 K, have been successfully simulated (53, 54), the magnetic properties of the Mn_4 moiety are poorly understood in the S_3 state, which precludes here a reliable simulation. Thus, to gain further insights into the structural reasons underlying these spectroscopic changes, we attempted to measure directly the EPR spectrum or $Tyr_Z^{\bullet}$.

Figs. 7-9 report the results of time-resolved EPR experiments performed at room temperature. The time resolution of our EPR spectrometer is in the same time range as the lifetime of $S_3Tyr_Z^{\bullet}$ in WT *T. elongatus* PSII ($t_{1/2}$ ~1 ms). To circumvent this limitation, Ca^{2+} and Cl^- were substituted by Sr^{2+} and Br^- in PsbA3-PSII because it has been shown that this markedly increases the lifetime of $S_3Tyr_Z^{\bullet}$ (39). In such conditions, the $S_3Tyr_Z^{\bullet}$ to S_0Tyr_Z transition occurs with a $t_{1/2}$ close to 7 ms (39),

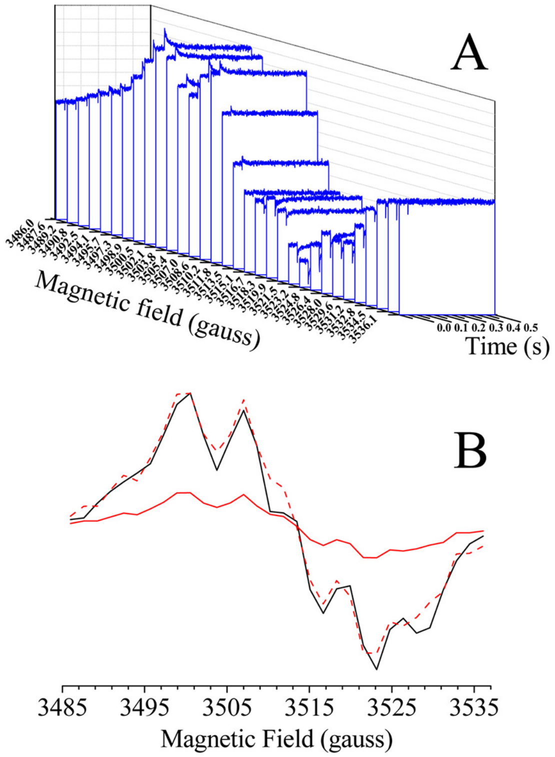

FIGURE 8. *A*, formation and decay of the $Tyr^{\bullet}$ signal following laser flash illumination of Sr/Br-PsbA3-PSII. The same protocol as in *panel A* of Fig. 7 was followed. *B*, spectra extracted from the two-dimensional spectra as explained for *panel B* of Fig. 7. The *black spectrum* corresponds to the $Tyr_Z^{\bullet}$ spectrum of manganese-depleted PsbA3-PSII, the *red spectrum* with a *continuous line* corresponds to the $Tyr_Z^{\bullet}$ spectrum of Sr/Br-PsbA3-PSII, and the *red spectrum* with a *dashed line* corresponds to the $Tyr_Z^{\bullet}$ spectrum of Sr/Br-PsbA3-PSII with an amplitude multiplied by four.

i.e. in a time domain compatible with the reliable detection of $Tyr_Z^{\bullet}$ decay with our EPR set-up. Because in separate experiments (not shown) we checked that the Cl^-/Br^- exchange had no effect on the $Tyr_Z^{\bullet}$ spectrum and because the Ca^{2+}/Sr^{2+} exchange alone proved sufficient to allow us the full detection of the $Tyr_Z^{\bullet}$ signal, the formation and decay of the $Tyr_Z^{\bullet}$ signals following laser flash illumination were done in Sr^{2+}-containing PsbA2-PSII. These measurements were done at 32 magnetic field positions spread over 50 G and centered on the $Tyr_Z^{\bullet}$ EPR spectrum.

To validate the approach, we first applied the method to manganese-depleted PSII in which the lifetime of $Tyr_Z^{\bullet}$ is much longer. Fig. 7*A* shows the results of such experiments, *i.e.* a two-dimensional spectrum (time *versus* field). Fig. 7*B* shows two slices extracted from the two-dimensional spectrum. The first one (*black spectrum*), before the flash, corresponds to the $Tyr_D^{\bullet}$ spectrum, and the second one (*red spectrum*), immediately after the flash and after subtraction of the baseline for each magnetic field value, corresponds to the $Tyr_Z^{\bullet}$ spectrum. Although the magnetic field resolution is here limited to 50/31 ~1.6 G, the $Tyr_D^{\bullet}$ and $Tyr_Z^{\bullet}$ spectra thus obtained are similar to those reported in the literature for manganese-depleted PSII (*e.g.* Refs. 46 and 55).

Fig. 8*A* shows the results of a similar two-dimensional experiment performed in Sr/Br-containing PsbA3-PSII. Here, in contrast to the situation prevailing in manganese-depleted PSII, the $Tyr_Z^{\bullet}$ signal was kinetically detectable only in the

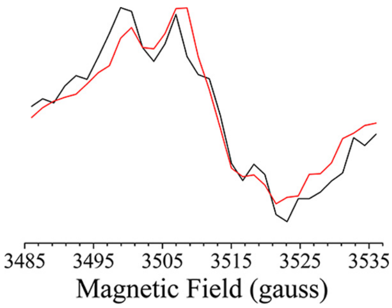

FIGURE 9. ***Black spectrum* corresponds to the $Tyr_Z^{\bullet}$ spectrum of Sr/Br-PsbA3-PSII, and *red spectrum* with a *dashed line* corresponds to the $Tyr_Z^{\bullet}$ spectrum of Sr-PsbA2-PSII.** Both spectra were extracted from a two-dimensional spectrum as explained above and correspond to the same Chl concentration and $Tyr_D^{\bullet}$ signal amplitude.

$S_3Tyr_Z^{\bullet}$ to S_0Tyr_Z transition. In addition, because 16 consecutive flashes were averaged for each sample, the amplitude of the $Tyr_Z^{\bullet}$ signal should be at most one-fourth of that detected in manganese-depleted PSII in which almost one $Tyr_Z^{\bullet}$ species is detectable upon each flash. Fig. 8*B* shows the $Tyr_Z^{\bullet}$ spectrum recorded in manganese-depleted PSII in Fig. 7 (*black spectrum*) and the $Tyr_Z^{\bullet}$ spectrum recorded immediately after the flash in Sr/Br-containing PsbA3-PSII (*red spectrum*, *solid line*). The latter has been multiplied 4-fold (*dashed red line*) to ease its comparison with the manganese-depleted case. Within experimental accuracy, the $Tyr_Z^{\bullet}$ spectrum in the $(S_3Tyr_Z^{\bullet})'$ state was found identical to the $Tyr_Z^{\bullet}$ spectrum in manganese-depleted PSII. In addition, we did not find any significant changes in the shape of the $Tyr_Z^{\bullet}$ spectrum occurring while it decays (see supplemental Figs. S3 and S4).

Finally, the two-dimensional EPR experiment was performed in Sr-containing PsbA2-PSII. Fig. 9 compares the $Tyr_Z^{\bullet}$ spectra detected in PsbA3-PSII (*black spectrum*) and that recorded in PsbA2-PSII (*red spectrum*) and evidences small but significant differences between the PsbA2-PSII and PsbA3-PSII $Tyr_Z^{\bullet}$ spectra in the $(S_3Tyr_Z^{\bullet})'$.

DISCUSSION

In this study, we describe for the first time the construction of a *T. elongatus* mutant in which both the *psbA$_1$* and the *psbA$_3$* genes have been deleted, so thus the mutant expresses only the *psbA$_2$* gene. The O_2-evolving activity of PSII purified from this strain is close to that measured with PsbA1-PSII (~3500 μmol of O_2 (mg of Chl)$^{-1}$ h^{-1}) and approximately half of that found for PsbA3-PSII (~6000 μmol of O_2 (mg of Chl)$^{-1}$ h^{-1}). In the current understanding, the limiting step of the overall oxygen evolution *in vitro* is the exchange of the doubly reduced Q_BH_2 molecule by an oxidized one. Thus, these different oxygen-evolving activities may stem from amino acid substitutions located close to the quinone binding sites. For example, in the x-ray three-dimensional structure of PsbA1-PSII[5] (3), S270 and C212 locate close to the Q_B binding site (supplemental Fig. S1). S270 is replaced by an alanine in both PsbA2-PSII and PsbA3-PSII, and C212 is by replaced by an alanine in PsbA2-PSII and a serine in PsbA3-PSII. However, sequence alignment does not permit the identification of other amino acids that would account for, on the one hand, the similarity between PsbA1-PSI and PsbA2-PSII and, on the other hand, the dissimilarities between these two and PsbA3-PSII. Probably, several amino acid substitutions between PsbA1-PSII, PsbA2-PSII, and PsbA3-PSII could potentially induce long distance effects acting on the hydrogen bond network, the water molecule network, the binding of lipids, and possibly the fine tuning of the interactions between the D1/D2 α-helices.

The C144P and P173M exchanges are two of the less conservative differences between PsbA2 and PsbA(1/3). In PsbA1 and PsbA3, the C144 is located in helix C on the periplasmic side just before the α-helix bearing Tyr_Z (the Y161), and the P173 is located in the loop between the C and D helices bearing Tyr_Z and the H190 (3) (see supplemental data). Many studies have documented the role and importance of this H-bond in determining the reaction pathway as well as the rate of the proton-coupled electron transfer process involved associated with the oxidation of Tyr_Z (*e.g.* Refs. 26, 30, and 31). Because its φ backbone dihedral angle is locked, proline is a singularly rigid amino acid. Its substitution for and by other residues in the vicinities of Tyr_Z and H190 is expected to have significant structural consequences on the local environment of Tyr_Z and therefore on this proton-coupled electron transfer. Therefore, it seems very likely that these substitutions have some consequences on the relative orientation of the Tyr_Z *versus* H190 and are therefore responsible for the changes reported in this work.

The period four oscillating pattern in PsbA2-PSII indicates that the miss parameter is larger than in either PsbA3-PSII (33, 39) or PsbA1-PSII (40) (Fig. 2). However, the yield of S_2 formation estimated from the amplitude of the S_2 EPR multiline signal was identical in PsbA2-PSII and PsbA3-PSII, thus showing that the yield of the S_1 to S_2 transition is not significantly affected (Fig. 4). In contrast, the smaller amplitude of the absorption change detected upon the second flash and the smaller S_3 EPR signal and the larger fraction of remaining S_2 multiline signal detected after two flashes applied to PSII centers synchronized in the S_1 state prior to the flash illumination suggest that in PsbA2-PSII, the miss parameter strongly increases in the S_2 to S_3 transition. The fact that the miss parameter depends on the S state transitions decreases the accuracy of a fitting of the period four oscillations in Fig. 2 (nevertheless, see supplemental Fig. S7 for a tentative fitting procedure). Based on the fraction of the remaining S_2 multiline signal, we estimate this increase to be 2-fold (*i.e.* ~20%).

The S_2 EPR multiline spectra and S_3 EPR spectra are known as being exquisitely sensitive to the structure and spin distribution within the cluster (41, 42). On the contrary, the absence of significant differences between these spectroscopic features obtained in the PsbA2-PSII and PsbA3-PSII show that the structure of the Mn_4CaO_5 is very likely not affected by the PsbA exchange. In addition, the $P_{680}{}^{+}/P_{680}$ difference spectra *versus* the flash number in PsbA2-PSII do not reveal any significant changes in the charge distribution over the $P_{D1}P_{D2}$ chlorophyll dimer because the spectra after one, two, or three flashes have a maximum bleaching at 433 nm as in PsbA1-PSII and PsbA3-PSII. Therefore, it seems likely that the increase of the miss

---

[5] The structure reported in Ref. 3 is from *T. vulcanus* and not from *T. elongatus*, which is used here. However the *psbA$_1$* genes, except for the threonine 286 in *T. elongatus* substituted for an alanine in *T. vulcanus*, are identical in the two organisms.

parameter reported above originates from a modification of Tyr_Z itself. Indeed, several authors have pointed to the electron transfer between Tyr_Z and P_{680} as being an important contributor to the miss parameter (for example, see Refs. 56–58 for discussions).

The similar kinetics observed for the $S_1Tyr_Z^{\bullet}$ to S_2Tyr_Z transition ($t_{1/2}$ ~50 μs), for whichever PsbA protein is involved, is consistent with an unmodified miss parameter on this transition. In the $S_3Tyr_Z^{\bullet}$ to S_0Tyr_Z transition, the decay of the $\Delta I/I$ at 292 nm is biphasic (Fig. 3). The fast phase ($t_{1/2}$ ~100 μs) seen as a lag phase at 292 nm has been interpreted as reflecting the electrostatically triggered expulsion of one proton from the catalytic center caused by the positive charge near/on $Tyr_Z^{\bullet}$ (59). The slow phase, attested by an absorption decay with $t_{1/2}$ ~1 ms, corresponds to the formation of S_0 and O_2 and to an additional proton release (Refs. 59–63), and see also Ref. 64 for a recent work dealing with this these two phases in *T. elongatus*). From data in Fig. 3, neither the lag phase $S_3Tyr_Z^{\bullet}$ to $(S_3Tyr_Z^{\bullet})'$ nor the $(S_3Tyr_Z^{\bullet})'$ to S_0Tyr_Z transition seems affected by the PsbA exchange.

For the $S_2Tyr_Z^{\bullet}$ to S_3Tyr_Z transition, in which EPR measurements clearly indicate an increase of the miss parameter, the measurements at 292 nm are unfortunately not very informative. Thus, to probe further the Tyr_Z environment, we measured the reduction of $P_{680}{}^{+}$. As previously observed by many groups (see below), this kinetics has multiple components. The fast ones have been interpreted as being kinetically limited by the electron transfer process and were similar in rates in the various samples. The phases developing in the μs to tens of μs time range have been interpreted as being kinetically limited by proton transfer, and these were markedly affected by the PsbA3 to PsbA2 exchange, in particular after the second and third flashes in the series. These components were slower, and their amplitudes were larger in PsbA2-PSII. This, together with the modified split EPR signal detected upon NIR illumination in PsbA2-PSII, shows that Tyr_Z is indeed the cofactor with modified properties in PsbA2-PSII. Before discussing these structural issues, we would like to note that as a side result of the present study, we report here the first $Tyr_Z^{\bullet}$ EPR spectrum in the $(S_3Tyr_Z^{\bullet})'$ state in active PSII. We show that it is similar to that in manganese-depleted PSII. From W-band EPR, the geometry of $Tyr_Z^{\bullet}$ in manganese-depleted PSII crystals was found to be similar to that expected from the geometry of Tyr_Z in the dark-adapted state of Mn_4CaO_5-containing crystal (65). Thus, the geometry of $Tyr_Z^{\bullet}$ in the $(S_3Tyr_Z^{\bullet})'$ state is also likely similar to that of Tyr_Z in the S_1 state.

Several structural reasons may be considered to account for the different properties of Tyr_Z. One is a change in the orientation of the $Tyr_Z^{\bullet}$ radical with respect to the Mn_4CaO_5 cluster that would modify the magnetic interaction between $Tyr_Z^{\bullet}$ and the Mn_4CaO_5 cluster. To further assess this, we attempted to characterize the g-tensor of $Tyr_Z^{\bullet}$ by high field EPR. We note, however, that this study was performed with manganese-depleted PsbA2-PSII (supplemental Fig. S5), so its conclusions cannot be straightforwardly extrapolated to oxygen-evolving PSII. Although small, the changes indicate without ambiguities that the g_x resonance of the $Tyr_Z^{\bullet}$ spectrum was broader and likely up-shifted. This could explain the modified X-band EPR spectrum measured in the $(S_3Tyr_Z^{\bullet})'$ state. An up-shift of the g_x value is indicative of a less positive electrostatic environment for $Tyr_Z^{\bullet}$ (47). The changes in the hyperfine structure of the time-resolved $Tyr_Z^{\bullet}$ spectrum in the $(S_3Tyr_Z^{\bullet})'$ state are also reminiscent of that observed in the $Tyr_D^{\bullet}$ spectrum in the D2-H189L mutant that disrupts the H-bond in which $Tyr_D^{\bullet}$ is involved (47). Altogether these data thus point to a weaker H-bond between Tyr_Z and H190.

The data above indicate that the main modifications on the electron donor side of PsbA2-PSII occur at the level of Tyr_Z. This could be a consequence of the C144P and P173M exchanges, which in turn would modify the H-bond between Tyr_Z and H190. It is indeed widely agreed that the proton-coupled electron transfer rates for the Tyr oxidation depend on the properties of the Tyr-O···H···N-His bonding (*e.g.* Refs. 26, 31, and 66). It has indeed been shown that, in model compounds, the proton-coupled electron transfer rate from a tyrosine to an oxidant was strongly dependent on the intramolecular distance between the tyrosine and the base that accepts the proton (*e.g.* Ref. 67). Interestingly, the hydrogen bond between the phenol group of Tyr_Z and the Nϵ of H190 in PSII is very short (2.46 Å in Ref. 3). Recently, the rationale underlying this short H-bond has been investigated by a quantum mechanical-molecular mechanical approach (68), and the cluster of four water molecules involved in the Mn_4CaO_5-Tyr_Z motif has been shown to play an important role in the stabilization of such a short distance. In this framework, it would not be surprising that a small distortion of such a delicate scaffold would have important consequences on the oxidation of Tyr_Z by $P_{680}{}^{+}$ and in particular on those steps that are kinetically limited by the proton transfer within the H-bond network in which Tyr_Z and His-190 are involved.

In contrast to the marked kinetic effects that we observed on the slow components of the oxidation of Tyr_Z by $P_{680}{}^{+}$, the reduction rates of the various $S_iTyr_Z^{\bullet}$ states were unaffected by the PsbA3 to PsbA2 exchange. As regards the S_1 to S_2 transition, this is expected because it is only accompanied by substoichiometric proton release (69–71). However, the subsequent S_2 to S_3 and S_3 to S_0 electron transfer steps are chemically coupled to proton release (*e.g.* Refs. 72 and 73) and might be affected by the changes in the H-bond network around Tyr_Z and His-190 discussed above. To our knowledge, the present study is the only one reporting a slowdown of the μs components in the oxidation of Tyr_Z besides, of course, the H/D experiments (43, 63, 74). Interestingly, kinetic isotope effects have also been reported for the following electron transfer step, *i.e.* the reduction of $Tyr_Z^{\bullet}$, at least in the presence of the S_2 and S_3 states. Notably, the most pronounced kinetic isotope effect has been reported to occur during the $S_3Tyr_Z^{\bullet}$ to $(S_3Tyr_Z^{\bullet})'$ (63), which is assigned to an electrostatically triggered proton release (59, 63). The present observation that the PsbA3 to PsbA2 exchange affects the μs components in the oxidation of $Tyr_Z^{\bullet}$ while keeping unaffected the proton release associated with the $S_3Tyr_Z^{\bullet}$ to $(S_3Tyr_Z^{\bullet})'$ transition suggests that this particular proton release does not originate from the same H-bond network as the one involved in the proton transfer triggered by the formation of $Tyr_Z^{\bullet}$. The latter has been described as a sequence of push-pull steps that would be initiated by the transfer of the phenolic proton from $\mathrm{Tyr_Z}$ to Nϵ of H190. The identity of the "proton releaser" during the $\mathrm{S_3Tyr_Z^{\bullet}}$ to $(\mathrm{S_3Tyr_Z^{\bullet}})'$ is not known, and several candidates have been considered. A substrate water molecule is an obvious one (for example, see Ref. 76 for a model in which both the proton and the electron originate from the substrate water molecule). Alternatively, it could be a protonated base, proposed to be CP43-R357 (77), that would undergo a pK_a shift upon the formation of the $\mathrm{S_3Tyr_Z^{\bullet}}\cdots\mathrm{HN}\epsilon(\mathrm{H190})^+$ state and would, by acting as a proton acceptor from water, promote water splitting. These different proton transfer events thus have essentially different mechanistic implications. Although one mainly reflects electrostatic relaxation, the other sets the stage for all the players in the water-splitting process. In such a framework, it is not surprising that they involve different molecular actors, and the present results support this expectation. Notably, they also point to a necessary conformational change to account for the fact that a new proton releaser that had stayed inactive until the formation of $\mathrm{S_3}$ would come into play when $\mathrm{S_3Tyr_Z^{\bullet}}\cdots\mathrm{HN}\epsilon(\mathrm{H190})^+$ is formed (for example, see Refs. 73 and 75 for experimental evidences of structural changes in the S state cycle).

REFERENCES

1. Ferreira, K. N., Iverson, T. M., Maghlaoui, K., Barber, J., and Iwata, S. (2004) Architecture of the photosynthetic oxygen-evolving center. *Science* **303,** 1831–1838
2. Guskov, A., Kern, J., Gabdulkhakov, A., Broser, M., Zouni, A., and Saenger, W. (2009) Cyanobacterial photosystem II at 2.9-Å resolution and the role of quinones, lipids, channels, and chloride. *Nat. Struct. Mol. Biol.* **16,** 334–342
3. Umena, Y., Kawakami, K., Shen, J. R., and Kamiya, N. (2011) Crystal structure of oxygen-evolving photosystem II at a resolution of 1.9 Å. *Nature* **473,** 55–60
4. Diner, B. A., and Rappaport, F. (2002) Structure, dynamics, and energetics of the primary photochemistry of photosystem II of oxygenic photosynthesis. *Annu. Rev. Plant. Biol.* **53,** 551–580
5. Renger, G. (2011) Light-induced oxidative water splitting in photosynthesis: energetics, kinetics, and mechanism. *J. Photochem. Photobiol. B* **104,** 35–43
6. Groot, M. L., Pawlowicz, N. P., van Wilderen, L. J., Breton, J., van Stokkum, I. H., and van Grondelle, R. (2005) Initial electron donor and acceptor in isolated photosystem II reaction centers identified with femtosecond mid-IR spectroscopy. *Proc. Natl. Acad. Sci. U.S.A.* **102,** 13087–13092
7. Holzwarth, A. R., Müller, M. G., Reus, M., Nowaczyk, M., Sander, J., and Rögner, M. (2006) Kinetics and mechanism of electron transfer in intact photosystem II and in the isolated reaction center: pheophytin is the primary electron acceptor. *Proc. Natl. Acad. Sci. U.S.A.* **103,** 6895–6900
8. Crofts, A. R., and Wraight, C. A. (1983) The electrochemical domain of photosynthesis. *Biochim. Biophys. Acta* **726,** 149–185
9. Velthuys, B. R., and Amesz, J. (1974) Charge accumulation at the reducing side of system 2 of photosynthesis. *Biochim. Biophys. Acta* **333,** 85–94
10. Kok, B., Forbush, B., and McGloin, M. (1970) Cooperation of charges in photosynthetic O_2 evolution-I. A linear four step mechanism. *Photochem. Photobiol.* **11,** 457–475
11. Joliot, P., and Kok, B. (1975) in *Bioenergetics of Photosynthesis* (Govindjee, ed) pp. 387–412, Academic Press, New York
12. Clarke, A. K., Soitamo, A., Gustafsson, P., and Oquist, G. (1993) Rapid interchange between two distinct forms of cyanobacterial photosystem II reaction-center protein D1 in response to photoinhibition. *Proc. Natl. Acad. Sci. U.S.A.* **90,** 9973–9977
13. Golden, S. S. (1995) Light-responsive gene expression in cyanobacteria. *J. Bacteriol.* **177,** 1651–1654
14. Komenda, J., Hassan, H. A., Diner, B. A., Debus, R. J., Barber, J., and Nixon, P. J. (2000) Degradation of the photosystem II D1 and D2 proteins in different strains of the cyanobacterium *Synechocystis* PCC 6803 varying with respect to the type and level of psbA transcript. *Plant Mol. Biol.* **42,** 635–645
15. Sicora, C. I., Appleton, S. E., Brown, C. M., Chung, J., Chandler, J., Cockshutt, A. M., Vass, I., and Campbell, D. A. (2006) Cyanobacterial psbA families in *Anabaena* and *Synechocystis* encode trace, constitutive, and UVB-induced D1 isoforms. *Biochim. Biophys. Acta* **1757,** 47–56
16. Kós, P. B., Deák, Z., Cheregi, O., and Vass, I. (2008) Differential regulation of psbA and psbD gene expression, and the role of the different D1 protein copies in the cyanobacterium *Thermosynechococcus elongatus* BP-1. *Biochim. Biophys. Acta* **1777,** 74–83
17. Mulo, P., Sicora, C., and Aro, E. M., (2009) Cyanobacterial psbA gene family: optimization of oxygenic photosynthesis. *Cell. Mol. Life Sci.* **66,** 3697–3710
18. Sicora, C. I., Ho, F. M., Salminen, T., Styring, S., and Aro, E. M. (2009) Transcription of a "silent" cyanobacterial psbA gene is induced by microaerobic conditions. *Biochim. Biophys. Acta* **1787,** 105–112
19. Sugiura, M., Kato, Y., Takahashi, R., Suzuki, H., Watanabe, T., Noguchi, T., Rappaport, F., and Boussac, A. (2010) Energetics in photosystem II from *Thermosynechococcus elongatus* with a D1 protein encoded by either the psbA1 or psbA3 gene. *Biochimica et Biophysica Acta* **1797,** 1491–1499
20. Nakamura, Y., Kaneko, T., Sato, S., Ikeuchi, M., Katoh, H., Sasamoto, S., Watanabe, A., Iriguchi, M., Kawashima, K., Kimura, T., Kishida, Y., Kiyokawa, C., Kohara, M., Matsumoto, M., Matsuno, A., Nakazaki, N., Shimpo, S., Sugimoto, M., Takeuchi, C., Yamada, M., and Tabata, S. (2002) Complete genome structure of the thermophilic cyanobacterium *Thermosynechococcus elongatus* BP-1. *DNA Res.* **9,** 123–130
21. Loll, B., Broser, M., Kós, P. B., Kern, J., Biesiadka, J., Vass, I., Saenger, W., and Zouni, A. (2008) Modeling of variant copies of subunit D1 in the structure of photosystem II from *Thermosynechococcus elongatus*. *Biol. Chem.* **389,** 609–617
22. Sander, J., Nowaczyk, M., Buchta, J., Dau, H., Vass, I., Deák, Z., Dorogi, M., Iwai, M., and Rögner, M. (2010) Functional characterization and quantification of the alternative PsbA copies in *Thermosynechococcus elongatus* and their role in photoprotection. *J. Biol. Chem.* **285,** 29851–29856
23. Kato, Y., Sugiura, M., Oda, A., and Watanabe, T. (2009) Spectroelectrochemical determination of the redox potential of pheophytin a, the primary electron acceptor in photosystem II. *Proc. Natl. Acad. Sci. U.S.A.* **106,** 17365–17370
24. Merry, S. A., Nixon, P. J., Barter, L. M., Schilstra, M., Porter, G., Barber, J., Durrant, J. R., and Klug, D. R. (1998) Modulation of quantum yield of primary radical pair formation in photosystem II by site-directed mutagenesis affecting radical cations and anions. *Biochemistry* **37,** 17439–17447
25. Cuni, A., Xiong, L., Sayre, R. T., Rappaport, F., and Lavergne, J. (2004) Modification of the pheophytin midpoint potential in photosystem II: modulation of the quantum yield of charge separation and of charge recombination pathways. *Phys. Chem. Chem. Phys.* **6,** 4825–4831
26. Rappaport, F., Boussac, A., Force, D. A., Peloquin, J., Brynda, M., Sugiura, M., Un, S., Britt, R. D., and Diner, B. A. (2009) Probing the coupling between proton and electron transfer in photosystem II core complexes containing a 3-fluorotyrosine. *J. Am. Chem. Soc.* **131,** 4425–4433
27. Sugiura, M., Iwai, E., Hayashi, H., and Boussac, A. (2010) Differences in the interactions between the subunits of photosystem II dependent on D1 protein variants in the thermophilic cyanobacterium *Thermosynechococcus elongatus*. *J. Biol. Chem.* **285,** 30008–30018
28. Boussac, A., Sugiura, M., and Rappaport, F. (2011) Probing the quinone binding site of photosystem II from *Thermosynechococcus elongatus* containing either PsbA1 or PsbA3 as the D1 protein through the binding characteristics of herbicides. *Biochim. Biophys. Acta* **1807,** 119–129
29. Ogami, S., Boussac, A., and Sugiura, M. (February 2, 2012) Deactivation processes in PsbA1-photosystem II and PsbA3-photosystem II under photoinhibitory conditions in the cyanobacterium *Thermosynechococcus elongatus*. *Biochim. Biophys. Acta* 10.1016/j.bbabio.2012.01.015
30. Debus, R. J. (2008) Protein ligation of the photosynthetic oxygen-evolving center. *Coord. Chem. Rev.* **252,** 244–258
31. Rappaport, F., and Lavergne, J. (2001) Coupling of electron and proton

transfer in the photosynthetic water oxidase. *Biochim. Biophys. Acta* **1503,** 246–259

32. Sugiura, M., and Inoue, Y. (1999) Highly purified thermo-stable oxygen-evolving photosystem II core complex from the thermophilic cyanobacterium *Synechococcus elongatus* having His-tagged CP43. *Plant Cell Physiol.* **40,** 1219–1231
33. Sugiura, M., Boussac, A., Noguchi, T., and Rappaport, F., (2008) Influence of histidine-198 of the D1 subunit on the properties of the primary electron donor, P680, of photosystem II in *Thermosynechococcus elongatus*. *Biochim. Biophys. Acta* **1777,** 331–342
34. Styring, S., and Rutherford, A. W. (1987) In the oxygen-evolving complex of photosystem II the S_0 state is oxidized to the S_1 state by D^+ (Signal-II slow). *Biochemistry* **26,** 2401–2405
35. Un, S., Dorlet, P., and Rutherford, A. W. (2001) A high field EPR tour of radicals in photosystems I and II. *Appl. Magn. Reson.* **21,** 341–361
36. Beal, D., Rappaport, F., and Joliot, P. (1999) A new high sensitivity 10-ns time-resolution spectrophotometric technique adapted to in vivo analysis of the photosynthetic apparatus. *Rev Sci Instrum.* **70,** 202–207
37. Lavergne, J. (1984) Absorption changes of photosystem II donors and acceptors in algal cells *FEBS Lett.* **173,** 9–14
38. Lavergne, J. (1991) Improved UV-visible spectra of the S-transitions in the photosynthetic oxygen-evolving system. *Biochim. Biophys. Acta* **1060,** 175–188
39. Ishida, N., Sugiura, M., Rappaport, F., Lai, T. L., Rutherford, A. W., and Boussac, A. (2008) Biosynthetic exchange of bromide for chloride and strontium for calcium in the photosystem II oxygen-evolving enzymes. *J. Biol. Chem.* **283,** 13330–13340
40. Sugiura, M., Rappaport, F., Brettel, K., Noguchi, T., Rutherford, A. W., and Boussac, A., (2004) Site-directed mutagenesis of *Thermosynechococcus elongatus* photosystem II: the O_2-evolving enzyme lacking the redox-active tyrosine D. *Biochemistry* **43,** 13549–13563
41. Cox, N., Rapatskiy, L., Su, J. H., Pantazis, D. A., Sugiura, M., Kulik, L., Dorlet, P., Rutherford, A. W., Neese, F., Boussac, A., Lubitz, W., and Messinger, J. (2011) Effect of Ca^{2+}/Sr^{2+} substitution on the electronic structure of the oxygen-evolving complex of photosystem II: a combined multifrequency EPR, 55Mn-ENDOR, and DFT study of the S_2 state. *J. Am. Chem. Soc.* **133,** 3635–3648
42. Boussac, A., Sugiura, M., Rutherford, A. W., and Dorlet, P. (2009) Complete EPR spectrum of the S_3 state of the oxygen-evolving photosystem II. *J. Am. Chem. Soc.* **131,** 5050–5051
43. Schilstra, M. J., Rappaport, F., Nugent, J. H., Barnett, C. J., and Klug, D. R. (1998) Proton/hydrogen transfer affects the S state-dependent microsecond phases of $P680^+$ reduction during water splitting. *Biochemistry* **37,** 3974–3981
44. Kuhn, P., Eckert, H., Eichler, H. J., and Renger, G. (2004) Analysis of the $P680^+$ reduction pattern and its temperature dependence in oxygen-evolving PSII core complexes from a thermophilic cyanobacteria and higher plants. *Phys. Chem. Chem. Phys.* **6,** 4838–4843
45. Christen, G., and Renger, G. (1999) The role of hydrogen bonds for the multiphasic $P680^+$ reduction by Y_Z in photosystem II with intact oxygen evolution capacity: analysis of kinetic H/D isotope exchange effects. *Biochemistry* **38,** 2068–2077
46. Tommos, C., Tang, X. S., Warncke, K., Hoganson, C. W., Styring, S., McCracken, J., Diner, B. A., and Bancock, G. T. (1995) Spin-density distribution, conformation, and hydrogen-bonding of the redox-active tyrosine $_{Y^{\cdot}Z}$ in photosystem II from multiple electron magnetic-resonance spectroscopies: implications for photosynthetic oxygen evolution. *J. Am. Chem. Soc.* **117,** 10325–10335
47. Un, S., Boussac, A., and Sugiura, M. (2007) Characterization of the tyrosine-Z radical and its environment in the spin-coupled $S_2Tyr_Z^{\bullet}$ state of photosystem II from *Thermosynechococcus elongatus*. *Biochemistry* **46,** 3138–3150
48. Ioannidis, N., and Petrouleas, V. (2000) Electron paramagnetic resonance signals from the S_3 state of the oxygen-evolving complex: a broadened radical signal induced by low temperature near-infrared light illumination. *Biochemistry* **39,** 5246–5254
49. Boussac, A., Sugiura, M., Kirilovsky, D., and Rutherford, A. W. (2005) Near-infrared-induced transitions in the manganese cluster of photosystem II: action spectra for the S_2 and S_3 redox states. *Plant Cell Physiol.* **46,** 837–842
50. Petrouleas, V., Koulougliotis, D., Ioannidis, N. (2005) Trapping of metalloradical intermediates of the S states at liquid helium temperatures: overview of the phenomenology and mechanistic implications. *Biochemistry* **44,** 6723–6728
51. Sanakis, Y., Ioannidis, N., Sioros, G., and Petrouleas, V. (2001) A novel $S = 7/2$ configuration of the manganese cluster of photosystem II. *J. Am. Chem. Soc.* **123,** 10766–10767
52. Boussac, A., Sugiura, M., Lai, T. L., and Rutherford, A. W. (2008) Low temperature photochemistry in photosystem II from *Thermosynechococcus elongatus* induced by visible and near-infrared light. *Philos. Trans. R Soc. Lond. B Biol. Sci.* **363,** 1203–1210
53. Dorlet, P., Boussac, A., Rutherford, A. W., and Un, U. (1999) Multifrequency high field EPR study of the interaction between the tyrosyl $_Z$ radical and the manganese cluster in plant photosystem II. *J. Phys. Chem. B* **103,** 10945–10954
54. Koulougliotis, D., Teutloff, C., Sanakis, Y., Lubitz, W., and Petrouleas, V. (2004) The $S_1Y_Z^{\bullet}$ metalloradical intermediate in photosystem II: an X- and W-band EPR study. *Phys. Chem. Chem. Phys.* **6,** 4859–4863
55. Mino, H., and Kawamori, A. (1994) Microenvironments of tyrosine D^+ and tyrosine Z^+ in photosystem II studied by proton matrix ENDOR. *Biochim. Biophys. Acta* **1185,** 213–220
56. Shinkarev, V. P., and Wraight, C. A. (1993) Oxygen evolution in photosynthesis: from unicycle to bicycle. *Proc. Natl. Acad. Sci. U.S.A.* **90,** 1834–1838
57. Lavergne, J., and Rappaport, F. (1998) Stabilization of charge separation and photochemical misses in photosystem II. *Biochemistry* **37,** 7899–7906
58. de Wijn, R., and van Gorkom, H. J. (2002) The rate of charge recombination in photosystem II. *Biochim. Biophys. Acta* **1553,** 302–308
59. Rappaport, F., Blanchard-Desce, M., and Lavergne, J. (1994) Kinetics of electron-transfer and electrochromic change during the redox transitions of the photosynthetic oxygen-evolving complex. *Biochim. Biophys. Acta* **1184,** 178–192
60. Koike, H., Hanssum, B., Inoue, Y., and Renger, G. (1987) Temperature dependence of S state transition in a thermophilic cyanobacterium, *Synechococcus vulcanus* copeland measured by absorption changes in the ultraviolet region. *Biochim. Biophys. Acta* **893,** 524–533
61. Razeghifard, M. R., and Pace, R. J. (1999) EPR kinetic studies of oxygen release in thylakoids and PSII membranes: a kinetic intermediate in the S_3 to S_0 transition. *Biochemistry* **38,** 1252–1257
62. Haumann, M., Liebisch, P., Müller, C., Barra, M., Grabolle, M., and Dau, H. (2005) Photosynthetic O_2 formation tracked by time-resolved x-ray experiments. *Science* **310,** 1019–1021
63. Gerencsér, L., and Dau, H. (2010) Water oxidation by photosystem II: H_2O-D_2O exchange and the influence of pH support formation of an intermediate by removal of a proton before dioxygen creation. *Biochemistry* **49,** 10098–10106
64. Rappaport, F., Ishida, N., Sugiura, M., and Boussac, A. (2011) Ca^{2+} determines the entropy changes associated with the formation of transition states during water oxidation by Photosystem II *Energ. Environ. Sci.* **4,** 2520–2524
65. Matsuoka, H., Shen, J. R., Kawamori, A., Nishiyama, K., Ohba, Y., and Yamauchi, S. (2011) Proton-coupled electron-transfer processes in photosystem II probed by highly resolved g-anisotropy of redox-active tyrosine Y_Z. *J. Am. Chem. Soc.* **133,** 4655–4660
66. Hays, A. M., Vassiliev, I. R., Golbeck, J. H., and Debus, R. J. (1999) Role of D_1-His-190 in the proton-coupled oxidation of tyrosine Y_Z in manganese-depleted photosystem II. *Biochemistry* **38,** 11851–11865
67. Zhang, M. T., Irebo, T., Johansson, O., and Hammarström, L. (2011) Proton-coupled electron transfer from tyrosine: a strong rate dependence on intramolecular proton transfer distance. *J. Am. Chem. Soc.* **133,** 13224–13227
68. Saito, K., Shen, J. R., Ishida, T., and Ishikita, H. (2011) Short hydrogen bond between redox-active tyrosine Y_Z and D_1-His-190 in the photosystem II crystal structure. *Biochemistry* **50,** 9836–9844
69. Forster, V., and Junge, W. (1985) Stoichiometry and kinetics of proton

release upon photosynthetic water oxidation. *Photochem. Photobiol.* **41,** 183–190

70. Rappaport, F., and Lavergne, J. (1991) Proton release during successive oxidation steps of the photosynthetic water oxidation process: stoichiometries and pH dependence. *Biochemistry* **30,** 10004–10012
71. Jahns, P., Lavergne, J., Rappaport, F., and Junge, W. (1991) Stoichiometry of proton release during photosynthetic water oxidation: a reinterpretation of the responses of neutral red leads to a noninteger pattern. *Biochim. Biophys. Acta* **1057,** 313–319
72. Lavergne, J., and Junge, W. (1993) Proton release during the redox cycle of the water oxidase. *Photosynth. Res.* **38,** 279–296
73. Dau, H., and Haumann, H. (2008) The manganese complex of photosystem II in its reaction cycle: basic framework and possible realization at the atomic level. *Coord. Chem. Rev.* **252,** 273–295
74. Christen, G., Seeliger, A., and Renger, G. (1999) P680^{+} reduction kinetics and redox transition probability of the water-oxidizing complex as a function of pH and H/D isotope exchange in spinach thylakoids. *Biochemistry* **38,** 6082–6092
75. Pushkar, Y., Yano, J., Sauer, K., Boussac, A., and Yachandra, V. (2008) Structural changes in the Mn_4Ca cluster and the mechanism of photosynthetic water splitting. *Proc. Natl. Acad. Sci. U.S.A.* **105,** 1879–1884
76. Westphal, K. L., Tommos, C., Cukier, R. I., and Babcock, G. T. (2000) Concerted hydrogen-atom abstraction in photosynthetic water oxidation. *Curr. Opin. Plant Biol.* **3,** 236–242
77. Sproviero, E. M., Gascón, J. A., McEvoy, J. P., Brudvig, G. W., and Batista, V. S. (2008) Quantum mechanics/molecular mechanics study of the catalytic cycle of water splitting in photosystem II. *J. Am. Chem. Soc.* **130,** 3428–3442